

Predicting the detectability of oscillations in solar-type stars observed by *Kepler*

W. J. Chaplin¹, H. Kjeldsen², T. R. Bedding³, J. Christensen-Dalsgaard², R. L. Gilliland⁴,
S. D. Kawaler⁵, T. Appourchaux⁶, Y. Elsworth¹, R. A. García⁷, G. Houdek⁸, C. Karoff²,
T. S. Metcalfe⁹, J. Molenda-Żakowicz¹⁰, M. J. P. F. G. Monteiro¹¹, M. J. Thompson⁹,
G. A. Verner^{12,1}, N. Batalha¹³, W. J. Borucki¹³, T. M. Brown¹⁴, S. T. Bryson¹³,
J. L. Christiansen¹⁵, B. D. Clarke¹⁵, J. M. Jenkins¹⁵, T. C. Klaus¹⁶, D. Koch¹³, D. An¹⁷,
J. Ballot¹⁸, S. Basu¹⁹, O. Benomar⁶, A. Bonanno²⁰, A.-M. Broomhall¹, T. L. Campante^{11,2},
E. Corsaro²⁰, O. L. Creevey^{21,22}, L. Esch¹⁹, N. Gai^{19,23}, P. Gaulme⁶, S. J. Hale¹,
R. Handberg², S. Hekker^{1,24}, D. Huber³, S. Mathur⁹, B. Mosser²⁵, R. New²⁶,
M. H. Pinsonneault²⁷, D. Pricopi²⁸, P.-O. Quirion²⁹, C. Régulo^{30,22}, I. W. Roxburgh¹²,
D. Salabert^{21,22}, D. Stello³, M. D. Suran²⁸

¹School of Physics and Astronomy, University of Birmingham, Edgbaston, Birmingham, B15 2TT, UK

²Department of Physics and Astronomy, Aarhus University, DK-8000 Aarhus C, Denmark

³Sydney Institute for Astronomy (SIfA), School of Physics, University of Sydney, NSW 2006, Australia

⁴Space Telescope Science Institute, Baltimore, MD 21218, USA

⁵Department of Physics and Astronomy, Iowa State University, Ames, IA 50011, USA

⁶Institut d’Astrophysique Spatiale, Université Paris XI – CNRS (UMR8617), Batiment 121, 91405 Orsay Cedex, France

⁷Laboratoire AIM, CEA/DSM – CNRS – Université Paris Diderot – IRFU/SAP, 91191 Gif-sur-Yvette Cedex, France

⁸Institute of Astronomy, University of Vienna, A-1180 Vienna, Austria

⁹High Altitude Observatory and, Scientific Computing Division, National Center for Atmospheric Research, Boulder, Colorado 80307, USA

¹⁰Astronomical Institute, University of Wrocław, ul. Kopernika, 11, 51-622 Wrocław, Poland

¹¹Centro de Astrofísica and Faculdade de Ciências, Universidade do Porto, Rua das Estrelas, 4150-762, Portugal

¹²Astronomy Unit, Queen Mary, University of London, Mile End Road, London, E1 4NS, UK

¹³NASA Ames Research Center, MS 244-30, Moffett Field, CA 94035, USA

¹⁴Las Cumbres Observatory Global Telescope, Goleta, CA 93117, USA

¹⁵SETI Institute/NASA Ames Research Center, MS 244-30, Moffett Field, CA 94035, USA

¹⁶Orbital Sciences Corporation/NASA Ames Research Center, Moffett Field, CA 94035, USA

¹⁷Ewha Womans University, 11-1 Daehyun-Dong Seodaemun-Gu, Seoul 120-750 Korea

¹⁸Institut de Recherche en Astrophysique et Planétologie, Université de Toulouse, CNRS, 14 av E. Belin, 31400 Toulouse, France

¹⁹Department of Astronomy, Yale University, P.O. Box 208101, New Haven, CT 06520-8101, USA

²⁰INAF Osservatorio Astrofisico di Catania, Via S.Sofia 78, 95123, Catania, Italy

²¹Departamento de Astrofísica, Universidad de La Laguna, E-38206 La Laguna, Tenerife, Spain

²²Instituto de Astrofísica de Canarias, E-38200 La Laguna, Tenerife, Spain

²³Beijing Normal University, Beijing 100875, P.R. China

²⁴Astronomical Institute, "Anton Pannekoek", University of Amsterdam, PO Box 94249, 1090 GE Amsterdam, The Netherlands

²⁵LESIA, CNRS, Université Pierre et Marie Curie, Université Denis Diderot, Observatoire de Paris, 92195 Meudon cedex, France

ABSTRACT

Asteroseismology of solar-type stars has an important part to play in the exoplanet program of the NASA *Kepler Mission*. Precise and accurate inferences on the stellar properties that are made possible by the seismic data allow very tight constraints to be placed on the exoplanetary systems. Here, we outline how to make an estimate of the detectability of solar-like oscillations in any given *Kepler* target, using rough estimates of the temperature and radius, and the *Kepler* apparent magnitude.

Subject headings: stars: oscillations — stars: interiors — stars: late-type

1. Introduction

The primary objective of the NASA *Kepler Mission* is to detect, by the transit method, Earth-sized planets in the habitable zones of solar-type main-sequence stars (Borucki et al. 2010; Koch et al. 2010). Photometry of most of the stars is conducted at a long cadence (LC) of 29.4 minutes, but a subset of up to 512 stars can be observed at a short cadence (SC) of 58.85 s. The exquisite precision and accuracy of the *Kepler* data mean they are also well suited to asteroseismic studies of stars (e.g., see Gilliland et al. 2010a, Jenkins et al. 2010). The cadence of the SC data is rapid enough to allow investigations of solar-like oscillations in solar-type stars, where dominant periods are of the order of several minutes (Chaplin et al. 2010, 2011a; Metcalfe et al. 2010).

Asteroseismology has an important role to play in the exoplanet program, in that the precise and accurate inferences on the stellar properties – i.e., radius, mass and age – that are made possible by the seismic data allow very tight constraints to be placed on the exoplanetary systems, e.g., tight estimation of the stellar radius constrains the size of the

²⁶Materials Engineering Research Institute, Faculty of Arts, Computing, Engineering and Sciences, Sheffield Hallam University, Sheffield, S1 1WB, UK

²⁷Department of Astronomy, The Ohio State University, 4055 McPherson Laboratory, 140 West 18th Avenue, Columbus, OH 43210, USA

²⁸Astronomical Institute of the Romanian Academy, Str. Cutitul de Argint, 5, RO 40557, Bucharest, RO

²⁹Canadian Space Agency, 6767 Boulevard de l’Aéroport, Saint-Hubert, QC, J3Y 8Y9, Canada

³⁰Departamento de Astrofísica, Universidad de La Laguna, E-38206 La Laguna, Tenerife, Spain

planet (Kjeldsen et al. 2009; Stello et al. 2009a; Christensen-Dalsgaard et al. 2010). Solar-type stars flagged as potential planet hosts are therefore prime candidates for asteroseismic study.

The LC lightcurves of solar-type stars that are flagged by the Transiting Planet Search pipeline as having significant transit-like features are modeled, and those stars having companion radii less than two Jupiter radii are labeled as a Kepler Object of Interest (KOI) (Batalha et al. 2010a). One of the factors that then determines whether or not to assign the star to one of limited number of SC slots – allowing more rapid time-cadence observations – is whether the intrinsic properties and the apparent magnitude of the star would allow the detection of solar-like oscillations. This paper describes the straightforward procedure that has been implemented to answer this question.

We use simple scaling relations to predict the oscillations and granulation properties of any given KOI. The predictions use as input basic information available on each star from the *Kepler Input Catalog* (or KIC; see, e.g., Batalha et al. 2010b). Together with the known apparent magnitude of a given target, the scaling relation predictions are used to construct an appropriate measure of the signal-to-noise ratio in the frequency-power spectrum of the solar-like oscillations, and, from that, we use some straightforward statistics to estimate the probability of detection for the star.

To calibrate and verify the recipe we use asteroseismic results on solar-type stars that were observed by *Kepler* during the first seven months of science operations. About 2000 stars, down to Kepler apparent magnitude $Kp \simeq 12.5$, were selected as potential solar-type targets based upon their KIC parameters. Each was observed for one month at a time in SC. Timeseries were prepared for asteroseismic analysis in the manner described by García et al. (2011), and different teams applied their codes to attempt to detect, and then extract the basic properties of, the solar-like oscillations. Several modeling teams also then applied codes to estimate the stellar properties – using the basic oscillations parameters as inputs – which we then also made use of in validation of the recipe.

The layout of the rest of the paper is as follows. We introduce in Section 2 the basic principles underlying the detection test. We then detail the scaling relation predictions that are required for the test: Section 3 gives the scaling relations for the solar-like oscillations, while Section 4 gives scaling relations for the granulation and shot-noise contributions to the background power spectral density. The various ingredients are brought together in Section 5, in which the test is described in detail. The predictions of the test are compared in Section 6 to real results returned on the solar-type ensemble that was observed for asteroseismology. We conclude by presenting some general predictions for detectability of *Kepler* KOIs.

2. Detection of solar-like oscillations

The frequency power spectra of solar-like oscillations in solar-type stars present a pattern of peaks with near regular frequency separations. The mode powers are modulated by an envelope. The envelope has a bell-shaped appearance in many stars for which solar-like oscillations have been observed (including the Sun). Different techniques have been devised and applied to the *Kepler* SC data to detect signatures of solar-like oscillations (e.g., see Chaplin et al. 2010; Campante et al. 2010; Hekker et al. 2010; Huber et al. 2009; Karoff et al. 2010; Mosser & Appourchaux 2009; Mathur et al. 2010; Roxburgh 2009). Some techniques rely on extracting signatures of the near-regular frequency separations of the oscillations; others search for signatures of the Gaussian-like power excess due to the oscillations.

Here, we devise and apply a simple statistical detection test that is based upon the second family of techniques. Our choice is predicated on the requirement that the test should be straightforward to implement on a large number of stars. Making an absolute prediction of the detectability of the frequency separations is more complicated than the test we adopt. Strictly speaking, it demands that the damping rates of the solar-like oscillations, and the rotation and angle of inclination of the star, are known. We therefore opt for a simpler approach, which does not require assumptions to be made about these properties. We do so in the knowledge that once the oscillations power excess has been detected, the large frequency separation in solar-type stars will also be readily extractable.

The detection test is based upon the total observed power due to p-mode oscillations in the star. Let P_{tot} be the total expected underlying mean power. As we shall show below, this is very easily estimated from scaling relations. In the frequency-power spectrum, the approximately Gaussian-shaped power envelope due to the oscillations sits on top of slowly varying background power, which we assume is dominated by contributions from shot/instrumental noise and stellar granulation. When the observed power in the oscillations relative to the background is high (i.e., high SNR), the power excess due to the oscillations will be clearly visible. However, at low SNR, statistical fluctuations in the background power may swamp the oscillations signal, so that the excess is much harder to see.

If B_{tot} measures the total underlying background power across the range in frequency occupied by the oscillations, then a “global” measure of SNR in the oscillations spectrum is given by

$$\text{SNR}_{\text{tot}} = P_{\text{tot}}/B_{\text{tot}}. \tag{1}$$

Provided SNR_{tot} is high enough, we may be able to claim an unambiguous detection of the power excess due to the oscillations. If N independent frequency bins have contributed to the estimation of the SNR, we may then test it against χ^2 $2N$ -d.o.f. statistics to determine

if the SNR is sufficiently high that it would be hard to explain by chance alone. This is a false-alarm approach.

Let us suppose that we demand that a false alarm test be passed at, say, the 1% level to merit a likely detection. We first estimate a false-alarm threshold, $\text{SNR}_{\text{thresh}}$, i.e., the SNR value above which there is less than a 1 in 100 chance of a χ^2 $2N$ -d.o.f. distribution giving a normalized value greater than or equal to this purely at random. We then use the scaling relations to estimate the expected underlying SNR_{tot} of the target, and, with that number in hand, we may then estimate the probability that an observed value of the SNR for the star would be greater than, or equal to, $\text{SNR}_{\text{thresh}}$, i.e., that it would pass the false-alarm test¹. This final probability serves as an estimate of the detection probability of the star.

3. Scaling relations for solar-like oscillations

3.1. ν_{max} and $\Delta\nu$

The frequency at the peak of the power envelope of the oscillations, where the observed modes present their strongest amplitudes, is commonly referred to as ν_{max} . Our ability to predict ν_{max} from the fundamental stellar properties allows us to estimate where in frequency the oscillations would be most prominent.

We assume that ν_{max} scales with the acoustic cut-off frequency (Brown et al. 1991; Kjeldsen & Bedding 1995) determined for an isothermal stellar atmosphere (as verified observationally by Mosser et al. 2010). This scaling has been shown to provide good predictions for observed solar-like oscillation spectra. This gives, in terms of the fundamental stellar properties, the following scaling relation:

$$\nu_{\text{max}} = \nu_{\text{max},\odot} \left(\frac{M}{M_{\odot}} \right) \left(\frac{R}{R_{\odot}} \right)^{-2} \left(\frac{T_{\text{eff}}}{T_{\text{eff},\odot}} \right)^{-0.5}, \quad (2)$$

where we have scaled against the solar values of $\nu_{\text{max},\odot} = 3150 \mu\text{Hz}$ and $T_{\text{eff},\odot} = 5777 \text{K}$.

The most striking characteristic frequency separations in the oscillation spectra are the so-called large frequency separations, $\Delta\nu$. These are the separations between consecutive overtones, n , having the same spherical angular degree, l . The average value of the large

¹If the underlying SNR_{tot} is greater than, or equal to, $\text{SNR}_{\text{thresh}}$ one might naively expect that the chances of passing the false-alarm test would be 100%. However, one must remember that the real observations will be modified by the χ^2 $2N$ -d.o.f. statistics, which will mean that not every case would pass.

frequency separation scales very well with the square root of the mean density of the star (e.g., see Christensen-Dalsgaard 1993). Here, we use this scaling and calibrate estimated values against the observed average large separation of the Sun, i.e.,

$$\Delta\nu = \Delta\nu_{\odot} \left(\frac{M}{M_{\odot}} \right)^{0.5} \left(\frac{R}{R_{\odot}} \right)^{-1.5}, \quad (3)$$

with $\Delta\nu_{\odot} = 134.9 \mu\text{Hz}$. It has also recently been shown (Stello et al. 2009b) that solar-like oscillations in main-sequence stars follow to good approximation the following relation:

$$\Delta\nu = \Delta\nu_{\odot} \left(\frac{\nu_{\text{max}}}{\nu_{\text{max},\odot}} \right)^{0.75}. \quad (4)$$

Use of Equation 4 allows us to eliminate M from Equations 2 and 3, to yield scaling relations that depend only on T_{eff} and R . The process of elimination yields the scaling relation $M \propto T_{\text{eff}}^{1.5}$, which is close to the relation $M \propto T_{\text{eff}}^{1.7}$ in Noyes et al. (1984). The scaling relations for $\Delta\nu$ and ν_{max} in R and T_{eff} are:

$$\nu_{\text{max}} = \nu_{\text{max},\odot} \left(\frac{R}{R_{\odot}} \right)^{-2} \left(\frac{T_{\text{eff}}}{T_{\text{eff},\odot}} \right), \quad (5)$$

$$\Delta\nu = \Delta\nu_{\odot} \left(\frac{R}{R_{\odot}} \right)^{-1.5} \left(\frac{T_{\text{eff}}}{T_{\text{eff},\odot}} \right)^{0.75}. \quad (6)$$

3.2. Mode amplitudes

In order to comment on mode detectability, we must be able to predict the mode amplitudes. We base our predictions on Kjeldsen & Bedding (1995) and Samadi et al. (2007). We make predictions for observations made in intensity (relevant to *Kepler* photometry). The prediction is that the maximum oscillation intensity amplitudes A_{max} of the radial ($l = 0$) modes scale like

$$A_{\text{max}} = A_{\text{max},\odot} \beta \left(\frac{L/L_{\odot}}{M/M_{\odot}} \right)^s \left(\frac{T_{\text{eff}}}{T_{\text{eff},\odot}} \right)^{-2}, \quad (7)$$

with the coefficient s often quoted between 0.7 and 1.0. We follow Kjeldsen & Bedding (1995), and assume that the temperature dependence is quadratic. We have also included another coefficient, β , because without any further correction the above relation is known to overestimate the amplitudes in the hottest solar-type stars (e.g., see Houdek 2006, and references therein). To estimate the solar RMS value $A_{\text{max},\odot}$ we used the *Kepler* response function in wavelength, and known measurements of the solar amplitudes made in narrow-band observations by the three wavelength channels of the VIRGO/SPM instrument onboard

SoHO (see Ballot, in preparation). From the SPM data we defined the observed solar amplitude as a function of wavelength, and then weighted this curve by the *Kepler* response function to give an estimated RMS value of $A_{\text{max},\odot} \sim 2.5$ ppm.

We have used results of *Kepler* observations of solar-type stars to calibrate the size of the correction β . Results on $\Delta\nu$ and ν_{max} were used by modeling teams, together with T_{eff} , to provide estimates of the stellar radii and masses (e.g., see Stello et al. 2009a; Basu et al. 2010; Quirion et al. 2010; Gai et al. 2010). These estimated stellar properties were used to calculate predicted maximum amplitudes using Equation 7, with the unknown (at this stage) β set to unity. We then calculated the ratios of the observed amplitudes, A_{max} (extracted by the Octave pipeline), to the predicted amplitudes, $(A_{\text{max}})_{\text{pred}}$, for different assumed values of s . We now go on to discuss the results obtained for $s = 1.0$.

The ratios for $s = 1.0$ are plotted in Fig. 1 against T_{eff} (left-hand panels) and $T_{\text{red}} - T_{\text{eff}}$ (right-hand panels). We define T_{red} to be the temperature on the red edge of the radial-mode δ -Scuti instability strip, given in Houdek et al. (1999), at the luminosity, L , of a given star:

$$T_{\text{red}} = T_{\text{red},\odot} (L/L_{\odot})^{-0.093} \quad (8)$$

with $T_{\text{red},\odot} = 8907$ K. Both panels of Fig. 1 show a decrease in the ratio of the observed to predicted amplitudes as T_{eff} increases. A more clearly defined trend is present in the $T_{\text{red}} - T_{\text{eff}}$ plot, and we therefore chose to use fits performed on these data to fix the correction β . We fitted the following functions: first

$$\beta = 1 - \exp\left(-\frac{T_{\text{red}} - T_{\text{eff}}}{\Delta T}\right), \quad (9)$$

and then the less restrictive

$$\beta = c_0 - c_1 \exp\left(-\frac{T_{\text{red}} - T_{\text{eff}}}{\Delta T}\right) \quad (10)$$

where c_0 , c_1 and ΔT were the free parameters to be optimized, and weights for the fits were fixed by the uncertainties on the amplitude ratios. The correction seeks to allow for the attenuation of the amplitudes at high T_{eff} (which maps to low $T_{\text{red}} - T_{\text{eff}}$), and since at progressively lower T_{eff} one expects the amplitude predictions to be much more robust, we require a function that turns over at high $T_{\text{red}} - T_{\text{eff}}$ (hence the choice of an exponential). The solid blue and dashed red lines in the right-hand panel of Fig. 1 show the best-fitting Equations 9 and 10, respectively. The best-fitting χ^2 for the two models were almost indistinguishable (about 2.3), and as such we chose to adopt the simpler Equation 9 as our model for β , with its best-fitting $\Delta T = 1550$ K. A fit to a simple straight-line model gave a marginally better χ^2 than either of the two exponential models. The straight-line

model does of course fail to capture the requirement that the amplitude ratio curve turn over at higher $T_{\text{red}} - T_{\text{eff}}$, and its use would lead to the prediction of unphysically high amplitudes in the coolest solar-type stars.

We also performed the above analyses assuming the predicted amplitudes scaled like $(L/M)^{0.7}$ (i.e., with $s = 0.7$ in Equation 7). However, we found that we had to increase arbitrarily our assumed value of $A_{\text{max},\odot}$ – from 2.5 to 3.1 ppm – otherwise most of the amplitude ratios lay significantly above unity. We therefore opted to fix $s = 1.0$ (as per the results outlined above).

To summarize, we have, using the scaling relations in R and T_{eff} , and taking $s = 1.0$,

$$A_{\text{max}} = 2.5 \beta \left(\frac{R}{R_{\odot}} \right)^2 \left(\frac{T_{\text{eff}}}{T_{\text{eff},\odot}} \right)^{0.5}, \quad (11)$$

with β calibrated by Equation 9 using $\Delta T = 1550$ K.

4. Scaling relations for background power spectral density

We assume that there are two dominant contributions to the background power spectral density in the vicinity of ν_{max} in the frequency-power spectrum. The largest contribution comes from instrumental/shot noise, which we define in terms of a simple offset b_{instr} . When observations of the oscillations are made in intensity, stellar granulation also contributes significant power which must be accounted for in estimation of the total background. We model the granulation power as a Lorentzian function centred on zero frequency (e.g., Harvey 1985), with a characteristic power spectral density, b_{gran} , and a characteristic timescale, τ_{gran} . The power spectral density P_{gran} at frequency ν_{max} is then given by:

$$P_{\text{gran}} = \frac{b_{\text{gran}}}{1 + (2\pi\tau_{\text{gran}}\nu_{\text{max}})^2} \text{ ppm}^2 \mu\text{Hz}^{-1}. \quad (12)$$

We now go on to describe scaling relations for each of the free parameters needed to model the total background, beginning with those describing the granulation term.

4.1. Scaling relations for stellar granulation

We follow Huber et al. (2009) in assuming that τ_{gran} scales inversely with ν_{max} , as proposed by Kjeldsen & Bedding (in preparation). This means that the denominator of Equation 12 will be constant for all stars. Taking solar values of $\tau_{\text{gran},\odot} = 210$ sec and

$\nu_{\max,\odot} = 3150 \mu\text{Hz}$, we have that:

$$P_{\text{gran}} \approx 0.055 b_{\text{gran}} \text{ ppm}^2 \mu\text{Hz}^{-1}. \quad (13)$$

To describe b_{gran} , we assume that the typical size of a convective granule is proportional to the scale height for an isothermal atmosphere, and that all granules behave in a statistically independent manner so that the total RMS fluctuation scales inversely as the square root of the number of observed granules. This leads to (e.g., Schwarzschild 1975; Kjeldsen & Bedding, in preparation; see also Baudin et al. 2006):

$$b_{\text{gran}} \propto \left(\frac{L}{L_{\odot}}\right)^2 \left(\frac{M}{M_{\odot}}\right)^{-3} \left(\frac{T_{\text{eff}}}{T_{\text{eff},\odot}}\right)^{-5.5}. \quad (14)$$

With $M \propto T_{\text{eff}}^{1.5}$ (see Section 3.1), the above implies that

$$\begin{aligned} P_{\text{gran}} \propto b_{\text{gran}} &\propto \left(\frac{R}{R_{\odot}}\right)^4 \left(\frac{T_{\text{eff}}}{T_{\text{eff},\odot}}\right)^{-2} \\ &\propto \left(\frac{\nu_{\max}}{\nu_{\max,\odot}}\right)^{-2}. \end{aligned} \quad (15)$$

We have tested Equation 15 using results from the *Kepler* survey on solar-type stars. The left-hand panel of Fig. 2 plots the best-fitting P_{gran} of solar-type stars with detected oscillations (given by a fit of a Harvey-like model, plus a flat offset, to the background power spectral density). The best-fitting power law is found to be $P_{\text{gran}} \propto \nu_{\max}^{-1.8}$, which is close to the prediction above. Using appropriate normalization from the real data, we therefore adopt:

$$P_{\text{gran}} \approx 0.1 \left(\frac{\nu_{\max}}{\nu_{\max,\odot}}\right)^{-2} \text{ ppm}^2 \mu\text{Hz}^{-1}. \quad (16)$$

The red line in Fig. 2 shows the prediction from Equation 16.

4.2. Scaling relations for instrumental/shot noise

We use the “minimal term” noise model for *Kepler* presented in Gilliland et al. (2010b) in order to predict the RMS noise, σ , per 58.85-sec integration in the time domain:

$$\sigma = \frac{10^6}{c} (c + 9.5 \times 10^5 (14/Kp)^5)^{1/2} \text{ ppm} \quad (17)$$

where $c = 1.28 \times 10^{0.4(12-Kp)+7}$ detections per cadence. The expected noise power spectral density in the frequency domain due to the instrumental noise is then given approximately by:

$$b_{\text{instr}} = 2 \times 10^{-6} \sigma^2 \Delta t \text{ ppm}^2 \mu\text{Hz}^{-1}, \quad (18)$$

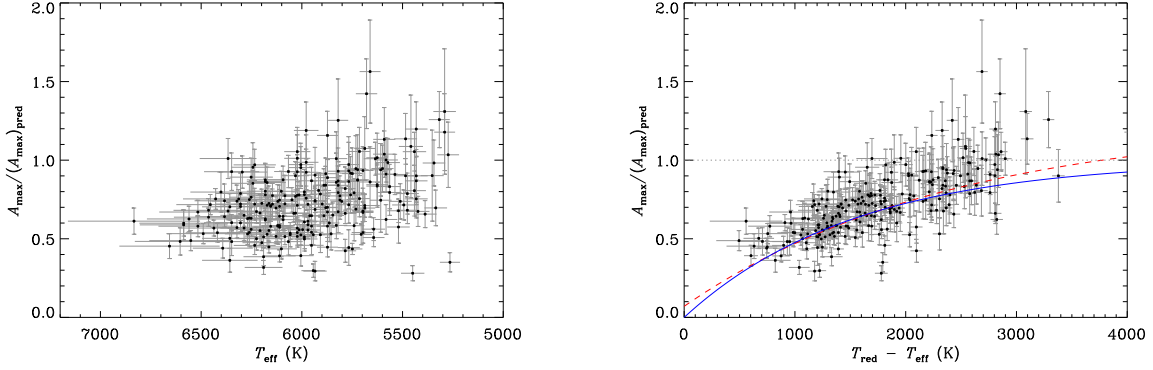


Fig. 1.— Plots of ratio of the observed to the predicted maximum mode amplitudes, assuming that the predicted amplitudes scale like $(L/M)^{1.0}$.

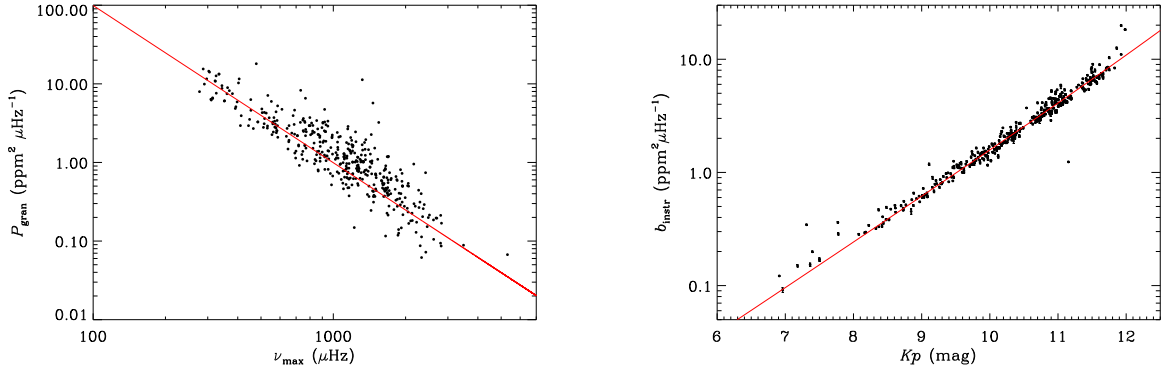


Fig. 2.— Left-hand panel: Best-fitting P_{gran} of solar-type stars observed by *Kepler* that showed oscillations. The line shows the prediction from Equation 16. Right-hand panel: Best-fitting b_{instr} of the same stars. The line shows the prediction from the minimal-term noise model in Gilliland et al. (2010b).

where Δt is the mean 58.85-sec cadence.

The right-hand panel of Fig. 2 plots the best-fitting b_{instr} of solar-type stars showing detected oscillations. The solid line shows the prediction from Equation 17. We see acceptable agreement between the observations and the predictions.

5. The detection test

5.1. Estimation of SNR_{tot}

First, we must compute the expected underlying global SNR of the target of interest, SNR_{tot} .

As noted previously, we assume that the power in the oscillations is modulated by a Gaussian-shaped envelope in frequency. We wish to calculate the total expected power underneath the envelope. The FWHM of the power envelope is assumed to be equal to $\nu_{\text{max}}/2$ (e.g., see Stello et al. 2007, and references therein; also Mosser et al. 2010), implying that most of the total mode power is contained within a range $\pm\nu_{\text{max}}/2$ around ν_{max} .

Each segment $\Delta\nu$ of the spectrum will contain power due to the visible $l = 0, 1, 2$ and 3 modes (although note that the relative contribution from the $l = 3$ modes is extremely weak). The $l = 0$ mode at the centre of the Gaussian-shaped envelope will have a power approximately equal to A_{max}^2 . The neighbouring $l = 1, 2$ and 3 modes in the central $\Delta\nu$ will contribute a further $\approx 2.1A_{\text{max}}^2$ of power (e.g., see Ballot, in preparation; Kjeldsen et al. 2008). This relative contribution is fixed by the relative visibilities of the different l . The total oscillations power in the central segment is therefore equal to $\approx 3.1A_{\text{max}}^2$.

To obtain the total mean power, P_{tot} , underneath the Gaussian-shaped envelope we must then add the contributions from all other segments of $\Delta\nu$ that fall in the range $\pm\nu_{\text{max}}/2$ around ν_{max} . In all, $\nu_{\text{max}}/\Delta\nu$ segments will contribute, with the average power of the contributing segments being ~ 0.5 times that of the central segment (the factor of 0.5 following from the fall-off in frequency of the Gaussian function). This implies that:

$$P_{\text{tot}} \approx 1.55A_{\text{max}}^2 \frac{\nu_{\text{max}}}{\Delta\nu}. \quad (19)$$

We must also make a correction for the fact that the high fractional duty cycle of the *Kepler* integrations, coupled with a cadence of nearly one minute, leads to apodization of the oscillations signal the closer ν_{max} is to the Nyquist frequency ($\sim 8496 \mu\text{Hz}$) of the SC

sampling. The amplitudes are suppressed by the factor

$$\eta = \text{sinc} \left[\pi/2 \left(\frac{\nu_{\text{max}}}{8496 \mu\text{Hz}} \right) \right], \quad (20)$$

so that Equation 19 should actually be written as

$$P_{\text{tot}} \approx 1.55 A_{\text{max}}^2 \eta^2 \frac{\nu_{\text{max}}}{\Delta\nu}. \quad (21)$$

Fig. 3 offers confirmation that Equation 21 does indeed provide a reasonably good description of P_{tot} , thereby implying that the Gaussian-envelope description provides a good model for the total observed oscillations power. It shows P_{tot} , as constructed with Equation 21 from the observed A_{max} , ν_{max} and $\Delta\nu$ of stars showing detected oscillations, against their actual measured P_{tot} , as given by the sum of the power excess above the fitted background in each frequency-power spectrum. The red line shows the one-to-one relation, which the data are seen to follow to good approximation.

We take one additional step for the detection recipe, and use Equations 5, 6 and 11 to re-express ν_{max} , $\Delta\nu$ and A_{max} in terms of R and T_{eff} , to give the following relation:

$$P_{\text{tot}} \approx 225 \text{ ppm}^2 \beta^2 \eta^2 \left(\frac{R}{R_{\odot}} \right)^{3.5} \left(\frac{T_{\text{eff}}}{T_{\text{eff},\odot}} \right)^{1.25}. \quad (22)$$

Turning next to the background, the total underlying background power in the frequency-power spectrum across the range ν_{max} is given approximately by:

$$B_{\text{tot}} \approx b_{\text{max}} \nu_{\text{max}}, \quad (23)$$

where b_{max} is the background power spectral density at the frequency ν_{max} , i.e.,

$$b_{\text{max}} = b_{\text{instr}} + P_{\text{gran}}. \quad (24)$$

For simplicity, we have ignored the frequency dependence of the background, assuming instead that the value b_{max} captures the average value of the background to sufficient accuracy. We may then calculate the global SNR in the total oscillations power as $\text{SNR}_{\text{tot}} = P_{\text{tot}}/B_{\text{tot}}$ (Equation 1).

5.2. Estimation of detection probability

A total of N independent frequency bins will contribute to estimation of the underlying P_{tot} and B_{tot} , and hence SNR_{tot} . We may therefore test SNR_{tot} against χ^2 $2N$ -d.o.f. statistics

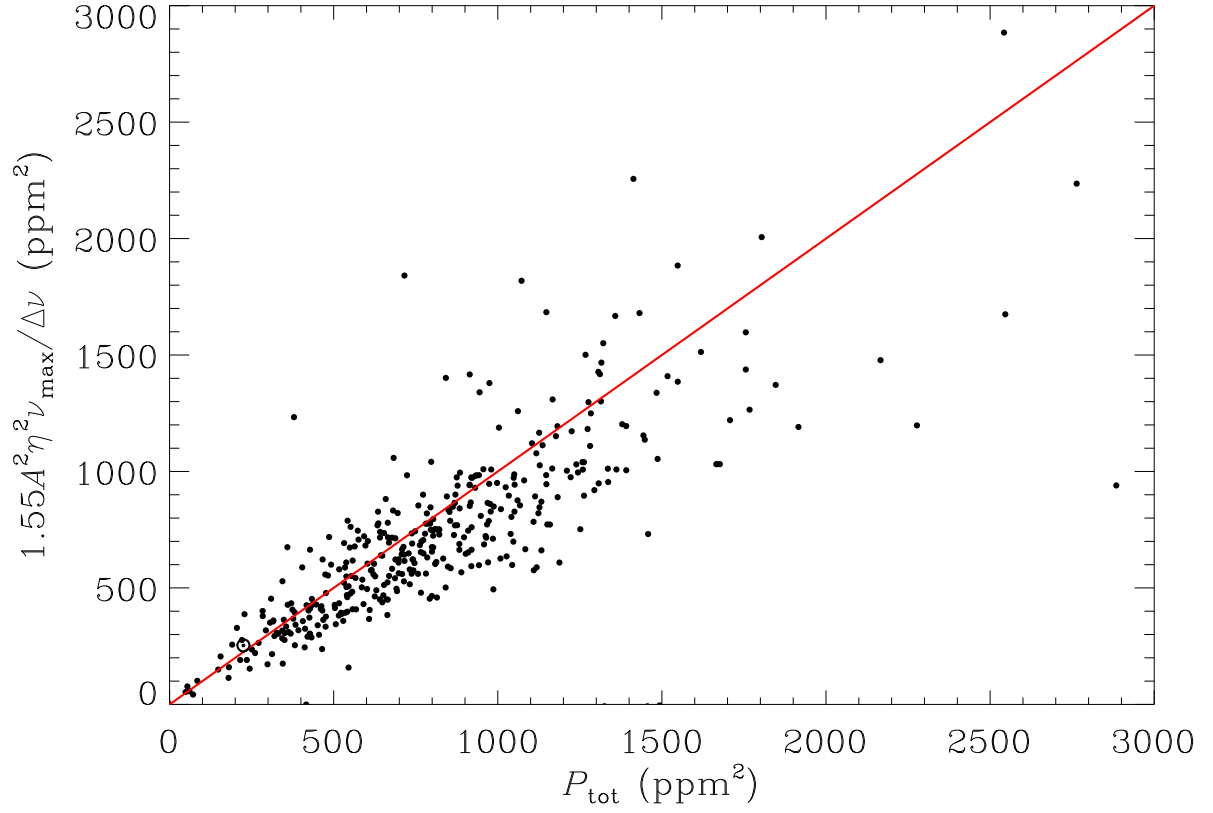


Fig. 3.— P_{tot} constructed with Equation 21 from the observed A_{max} , ν_{max} and $\Delta\nu$ of the stars showing detected oscillations against the actual measured P_{tot} given by the sum of the power excess above the fitted background of each frequency-power spectrum.

to determine if the observed SNR would be large enough that it would be hard to explain by chance alone. If T is the length of the timeseries, then N will be given by:

$$N = \left(\frac{\nu_{\max}/\mu\text{Hz} \times T/\text{sec}}{10^6} \right). \quad (25)$$

The probability of obtaining any value SNR' above a given level SNR is given by:

$$P(\text{SNR}' \geq \text{SNR}, N) = \int_x^\infty \frac{\exp(-x')}{\Gamma(N)} x'^{(N-1)} dx', \quad (26)$$

where $x = 1 + \text{SNR}$ and Γ is the Gamma function. Note the normalization of x : as SNR tends to zero (i.e., no oscillation signal present), we demand that x tends to unity.

To flag a possible detection, we would demand that the *observed* SNR of the star exceed some SNR threshold, $\text{SNR}_{\text{thresh}}$, corresponding to a fractional false-alarm probability, p (e.g., $p = 0.01$, or 1%). The required false-alarm threshold follows by solving:

$$P(\text{SNR}' \geq \text{SNR}_{\text{thresh}}, N) = p. \quad (27)$$

The probability that the observed SNR would exceed $\text{SNR}_{\text{thresh}}$ is then given by

$$P_{\text{final}} = \int_y^\infty \frac{\exp(-y')}{\Gamma(N)} y'^{(N-1)} dy', \quad (28)$$

with

$$y = (1 + \text{SNR}_{\text{thresh}})/(1 + \text{SNR}_{\text{tot}}). \quad (29)$$

We may regard P_{final} as providing an approximate estimate of the probability of detecting solar-like oscillations in the star. The equation for N captures the sensitivity of the detection probability to the length of the observations, T . As T , and hence N , increases, so the relative statistical fluctuations in B_{tot} will decrease in magnitude; hence, for a given underlying SNR_{tot} , the excess power due to the oscillations will be more clearly visible against the background (as reflected in a reduction in the size of $\text{SNR}_{\text{thresh}}$).

6. Results

We now apply our detection test to the solar-type stars observed for one month each by *Kepler* during the first seven months of science operations. We use the KIC R and T_{eff} and apparent magnitude of each target to predict whether oscillations would be detectable in one month. We then compare our predictions, in a statistical sense, with the actual results from

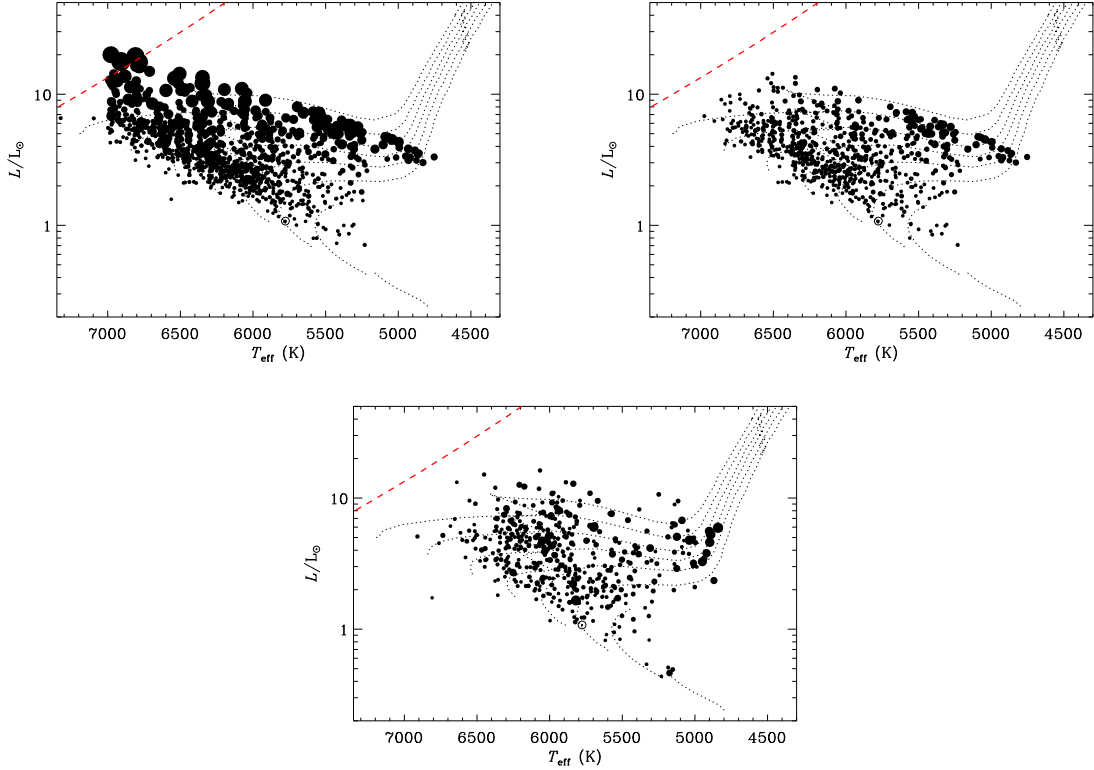


Fig. 4.— Bottom panel: H-R diagram of stars that showed detections of solar-like oscillations in their *Kepler* Q1, Q2 or Q3 survey data. Symbol size is proportional to SNR_{tot} . The location of the Sun is marked with the usual solar symbol. The dotted lines are evolutionary tracks (Padova models) for solar composition, computed for masses ranging from 0.7 to $1.5 M_{\odot}$ (see text). The dashed red line marks the approximate location of the red edge of the instability strip. Top left-hand panel: Predictions based on KIC parameters of all observed solar-type targets, but without the β correction, showing stars for which $P_{\text{final}} \geq 0.9$. Top right-hand panel: Predictions after application of the β correction to the scaling relation for the oscillation amplitudes.

Kepler. We only consider stars having an observed, or predicted, $\nu_{\max} \geq 350 \mu\text{Hz}$, which takes us approximately to the base of the red-giant branch.

The bottom panel of Fig. 4 plots stars that showed detections of solar-like oscillations with $\nu_{\max} \geq 350 \mu\text{Hz}$, with luminosities estimated from the seismically determined radii. We demanded that at least two of the asteroseismic data analysis pipelines returned consistent results on a star, giving a total of 499 stars with flagged detections. This is out of a total of 1750 observed stars having predicted $\nu_{\max} \geq 350 \mu\text{Hz}$. The sizes of the symbols are proportional to the observed SNR_{tot} . The dotted lines in Fig. 4 are evolutionary tracks (Padova models; Giradi et al. 2002, 2004; Marigo et al. 2008) computed for solar composition and masses ranging from 0.7 to $1.5 M_{\odot}$ in steps of $0.1 M_{\odot}$. The dashed red line marks the location of the red edge of the instability strip (for fundamental radial-mode δ -Scuti pulsations; see Houdek et al. 1999). The Sun is plotted with its usual symbol. The lack of detections close to the red edge, along with the amplitude ratio data plotted in Fig. 1, will provide important inputs for modeling the excitation and damping of solar-like oscillations (i.e., the interplay between those oscillations and the convection).

The top panels in Fig. 4 show results from the predictions, which were made using the KIC parameters of the stars, and only stars for which $P_{\text{final}} \geq 0.9$ were plotted. (Note that here the luminosities were estimated from the KIC parameters – using the radius and T_{eff} – whereas the luminosities in the lower panel are the observed luminosities, from the seismically determined radii and T_{eff} .) Symbol sizes are proportional to the *predicted* SNR_{tot} . The top left-hand panel shows predictions *without* the β correction having been applied. A total of 1163 stars are flagged with predicted detections. This emphasizes the importance of applying the β correction, since without it the predicted detections run all the way to the red-edge of the instability strip, and the predicted SNR_{tot} reach noticeably higher values across the ensemble than do the real observations. When the β correction is applied, we obtain the results plotted in the top right-hand panel. There is now much better agreement with the observations, and 765 stars are flagged with predicted detections.

Fig. 5 shows histograms of the observed detections (solid red lines), the β -corrected predictions (dashed blue lines), and the total number of observed stars having predicted $\nu_{\max} \geq 350 \mu\text{Hz}$ (dotted lines), as functions of KIC apparent magnitude, Kp (left-hand panel) and KIC T_{eff} (right-hand panel). We see good agreement between the distributions of observed detections and β -corrected predictions.

The predicted number of detections exceeds the observed number by about 50%. Several factors contribute to this overestimation. First, it turns out that there are several classical oscillators in the ensemble. The KIC parameters imply that these stars should show detectable solar-like oscillations; however, owing to uncertainties in the categorization it appears that

they are actually too hot. Second, there are several eclipsing binaries in the sample, which can make automated extraction of the oscillations parameters more challenging (due to the presence of fairly sharp features in the lightcurves). Neither of the above categories of stars is sufficiently numerous or troubling to account for most of the overestimation. It appears instead that elevated levels of stellar activity might be responsible for suppression of the mode amplitudes, and hence levels of detectability, in a sufficient number of stars to possibly explain the mismatch (as reported in Chaplin et al. 2011b). This may also relate to an interesting difference between the predictions and observations in the set of stars covering $6 \lesssim L/L_{\odot} \lesssim 9$ and $5300 \lesssim T_{\text{eff}} \lesssim 5700$ K in the upper right-hand panel of Fig. 4, which are largely missing from the lower panel. Gilliland (1985) has noted that stars in this region may show interesting evolutionary effects in their stellar dynamos, which would manifest themselves in the surface magnetic activity. We also add a note of caution regarding stars in this part of the H-R diagram. They have $\nu_{\text{max}} \sim 350$ to ~ 500 μHz . This range in frequency coincides with an instrumental artefact in the *Kepler* data (see García et al. 2010), which may hamper detection of the solar-like oscillations.

We finish by using the detection test to predict the detection probabilities for four canonical main-sequence stars: early-type and late-type K stars, the Sun (late G), and a mid-type F star. Fig. 6 plots the detection probabilities, P_{final} , for different assumed lengths of observation, T (see figure annotation), as a function of *Kepler* apparent magnitude, Kp . The detection rates fall off quite sharply with Kp , and long timescale observations are required in order to detect oscillations in stars fainter than $Kp \sim 13$.

Funding for this Discovery mission is provided by NASA’s Science Mission Directorate. The authors wish to thank the entire *Kepler* team, without whom these results would not be possible. We also thank all funding councils and agencies that have supported the activities of KASC Working Group 1. WJC, YE, SJH and GAV acknowledge the support of the UK Science and Technology Facilities Council (STFC). SH acknowledges support from the Netherlands Organisation for Scientific Research (NWO). NCAR is supported by the National Science Foundation. We are also grateful for support from the International Space Science Institute (ISSI).

REFERENCES

- Basu, S., Chaplin, W. J., Elsworth, Y., 2010, ApJ, 710, 1596
- Batalha, N. M., Rowe, J. F., Gilliland R. L., et al., 2010a, ApJ, 713, L97

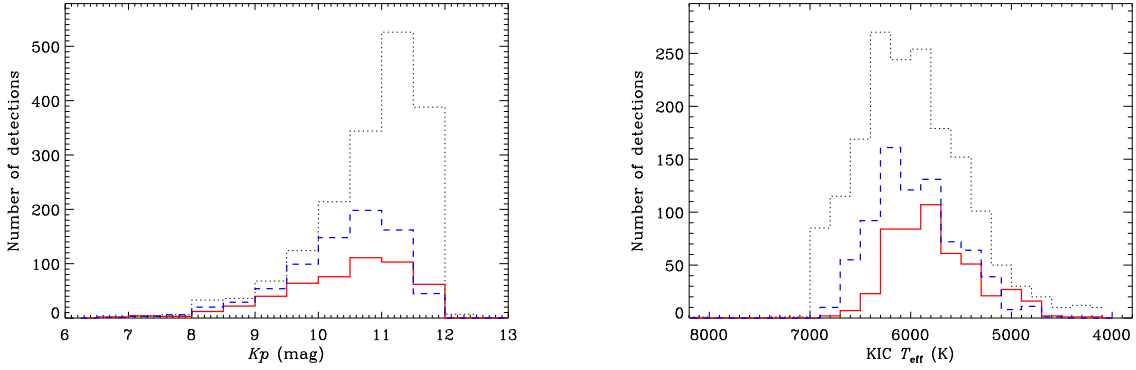


Fig. 5.— Histograms of the observed detections (solid red lines), the β -corrected predictions (dashed blue lines), and the total number of observed stars having predicted $\nu_{\max} \geq 350 \mu\text{Hz}$ (dotted lines), as functions of KIC apparent magnitude, Kp (left-hand panel) and KIC T_{eff} (right-hand panel).

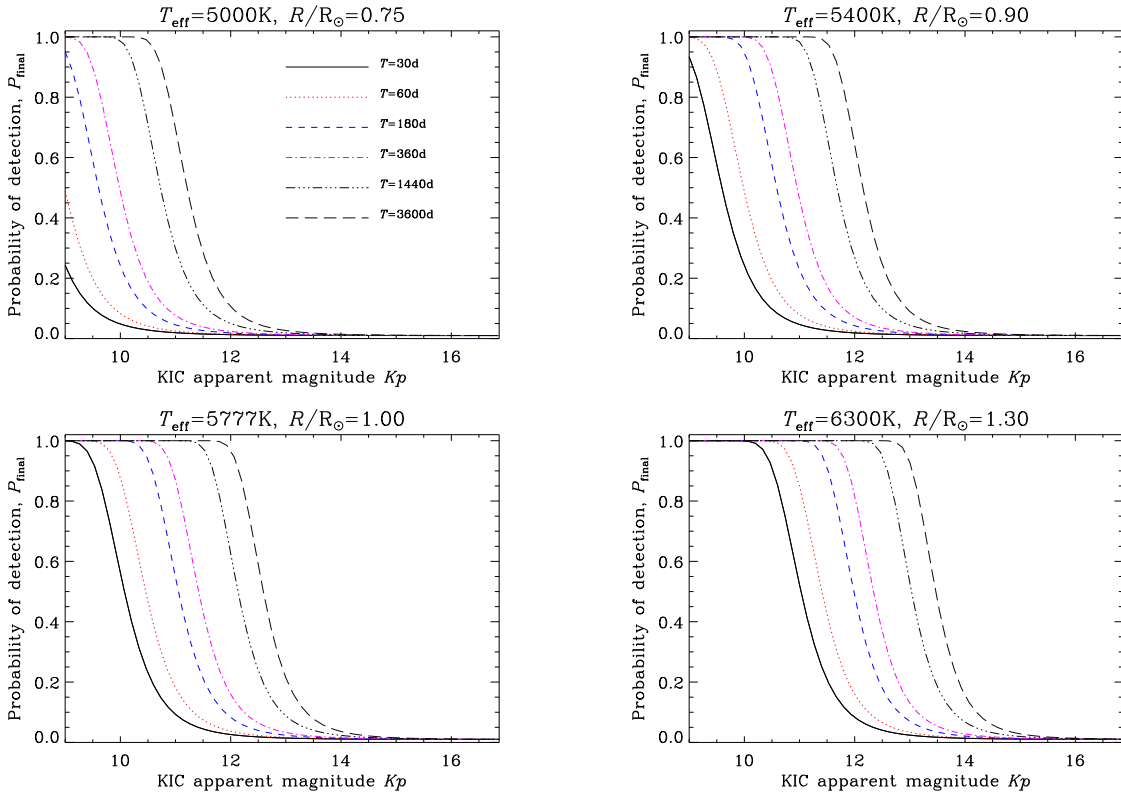


Fig. 6.— Detection probabilities, P_{final} , of four different main-sequence stars for different assumed lengths of observation, T (see anotation) as a function of *Kepler* apparent magnitude, Kp

- Batalha, N. M., Rowe, J. F., Gilliland R. L., et al., 2010b, *ApJ*, 713, L109
- Baudin, F., Samadi, R., Appourchaux, T., Michel, E., 2006, in: *Proceedings of The CoRoT Mission Pre-Launch Status – Stellar Seismology and Planet Finding (ESA-SP 1306)*, eds. M. Fridlund, A. Baglin, J. Lochard, L. Conroy, p. 403
- Borucki, W. J., Koch, D. G., Basri, G., et al., 2010, *Sci*, 327, 977
- Brown, T. M., Gilliland, R. L., Noyes, R. W., Ramsey, L. W., 1991, *ApJ*, 368, 599
- Campante, T. L., Karoff, C., Chaplin, W. J., Elsworth, Y., Handberg, R., Hekker, S., 2010, *MNRAS*, 408, 542
- Chaplin, W. J., Appourchaux, T., Elsworth, Y., et al., 2010, *ApJ*, 713, L169
- Chaplin, W. J., Kjeldsen, H., Christensen-Dalsgaard, J., et al., 2011a, *Science*, in the press
- Chaplin, W. J., Bedding, T. R., Bonanno, A., et al., 2011b, *ApJ*, submitted
- Christensen-Dalsgaard J., 1993, in: T. M. Brown (ed.), *Proc GONG 1992: Seismic Investigation of the Sun and Stars*, ASP. Conf. Ser. vol. 42 (San Francisco ASP), 347
- Christensen-Dalsgaard, J., Kjeldsen, H., Brown, T. M., et al., 2010, *ApJ*, 713, L164
- Gai, N., Basu, S., Chaplin, W. J., Elsworth, Y., 2011, *ApJ*, in the press (arXiv:1010.0834)
- García, R. A., Hekker, S., Stello, D., et al., 2011, *MNRAS*, in the press
- Gilliland, R. L., 1985, *ApJ*, 299, 286
- Gilliland, R. L., Brown, T. M., Christensen-Dalsgaard, J., et al., *PASP*, 2010a, 122, 131
- Gilliland, R. L., Jenkins, J. M., Borucki, W. J., et al., 2010b, *ApJ*, 713, 160L
- Giradi, L., Bertelii, G., Bressnan, A., Chiosi, C., Grönnewegen, M. A. T., Marigo, P., Salasnich, B., Weiss, A., 2002, *A&A*, 391, 195
- Giradi, L., Grebel, E., K., Odenkirchen, M., Chiosi, C., 2004, *A&A*, 422, 205
- Harvey, J., 1985, in: *Future Missions in Solar, Heliospheric and Space Plasma Physics*, ESA Workshop, eds. E. Rolfe, B. Battrick, Noordwijk, Netherlands, p. 199
- Hekker, S., Broomhall, A.-M., Chaplin, W. J., et al., 2010, *MNRAS*, 402, 2049
- Houdek, G., Balmforth, N., J., Christensen-Dalsgaard, J., Gough, D. O., 1999, *A&A*, 351, 582

- Houdek G., 2006, in: Beyond the Spherical Sun, SOHO18/GONG 2006/HELAS I, eds. D. Dansey, M. J. Thompson, ESA SP-624, Sheffield, UK, p. 28.1
- Huber, D., Stello, D., Bedding, T. R., et al., 2009, *CoAst*, 160, 74
- Jenkins, J. M., Caldwell, D. A., Chandraekaren, H., et al., 2010, *ApJ*, 713, L87
- Karoff, C., Campante, T. L., Chaplin, W. J., 2010, *AN*, in the press
- Kjeldsen, H., Bedding, T. R., 1995, *A&A*, 293, 87
- Kjeldsen, H., Bedding, T. R., Arentoft, T., et al., 2008, *ApJ*, 682, 1370
- Kjeldsen, H., Bedding, T. R., Christensen-Dalsgaard, J., 2009, in *IAU Symp. 253, Transiting Planets*, ed. F. Pont, D. Sasselov, M. Holman (Cambridge: Cambridge Univ. Press)
- Koch, D. G., Borucki, W. J., Basri, G., et al., 2010, *ApJ*, 713, L79
- Marigo, P., Girardi, L., Bressan, A., et al. 2008, *A&A*, 482, 883
- Mathur, S., García, R. A., Régulo C., et al., 2010, *A&A*, 511, 46
- Metcalf, T. S., Monteiro M. J. P. F. G., Thompson, M. J., et al., 2010, *ApJ*, 723, 1583
- Mosser, B., Appourchaux, T., 2009, *A&A*, 508, 877
- Mosser, B., Belkacem, K., Goupil, M.-J., et al., 2010, *A&A*, 517, 22
- Noyes, R. W., Hartmann, L. W., Baliunas, S. L., Duncan, D. K., Vaughan, A. H., 1984, *ApJ*, 279, 763
- Quirion, P.-O., Christensen-Dalgaard, J., Arentoft, T., 2010, *ApJ*, 725, 2176
- Roxburgh, I. W., 2009, *A&A*, 506, 435
- Samadi, R., Georgobiani, D., Trampedach, R., Goupil, M. J., Stein, R. F., Nordlund, A., 2007, *A&A*, 463, 297
- Schwarzschild, M., 1975, *ApJ*, 195, 137
- Stello, D., Bruntt, H., Kjeldsen, H., et al., 2007, *MNRAS*, 377, 584
- Stello, D., Chaplin, W. J., Bruntt, H., et al., 2009a, *ApJ*, 700, 1589
- Stello, D., Chaplin, W. J., Basu, S., Elsworth, Y., Bedding, T. R., 2009b, *MNRAS*, 400, L80